Journal of Civil Engineering (IEB), 39 (2) (2011) 135-148

Journal of Civil Engineering IEB

Numerical simulation of dead zone flows in an open channel with a side cavity and sudden enlargement

Md. Shahjahan Ali[1], Tanziha Mahjabin and Sadia Jahan Ria

Department of Civil Engineering,
Khulna University of Engineering and Technology, Khulna 9203, Bangladesh

Received 28 August 2011

Abstract

Three–dimensional numerical simulation is carried out to study the fundamental properties of flows in an open channel with a dead zone. In this paper, the flow field in two types of dead zone have been studied: one is rectangular side cavity and another one is the dead zone created at the downstream of channel with width enchroachment (i.e. sudden enlarged zone). A non-linear k-ε model is employed using finite volume method with a curvilinear coordinate system. It is found that the flow in the side cavity is characterized by three types of flow phenomena: the circulation inside the dead-zone, periodic coherent vortices at the interface of main stream and dead zone, and the water surface oscillation inside the dead zone. In this study all these characteristics are successfully reproduced by numerical simulation. The time averaged flow properties and temporal change of velocity profiles are well compared with previous experimental results. With increasing the length of the cavity, the circulation pattern and their numbers are changed along with velocity magnitude. For the open channel with sudden enlargment, although the upstream arrangemnet of flow domain is same as the cavity flow, the flow in the enlarged zone has the freedom to flow towards downstream in logitudinal direction. Due to this free downstream, the simulated flow field in the sudden enlarged zone is significantly different than that of open channel flows with side cavity. Beside the academic interests, present study contributes to understand the developement, extent and behaviour of flows in a dead zone for proper managemnet of river system and other water courses.

Keywords: Open channel flow, dead-zone, side cavity, sudden enlargement, Unsteady RANS, non-linear k–ε model

1. Introduction

The floodplain encroachment in a river is generally created due to construction of hydraulic structures such as embayment, spur-dykes etc. along the river for flood protection, navigation, bank protection, protection of bridges etc. The obstructed flow field in the downstream of a single spur-dyke or the flow field enclosed by two consecutive groynes are low velocity region compared to mainstream. This type of zone is generally termed as dead-zone. Flow velocity inside such kind of arrangement is lower than main channel. In addition to engineering applications, such structures increase the biodiversity of aquatic species by creating habitat and providing shelter for them. The main stream of a river, where the velocity is high, is not suitable for weak and small fishes. That's why the dead zone is a suitable shelter for them. In this study the flow field in two types of dead zone have been studied: one is rectangular side cavity and another one is the dead zone created at the downstream of channel with width encroachment (i.e. sudden enlarged zone).

1.1 Rectangular side cavity

It is an enclosed portion in a side of open channel where there is no longitudinal flow from upstream and no downstream flow from the cavity; the flow enters laterally from the main stream and there is a lateral interchange of flow between mainstream and cavity. Figure 1 shows two field photographs of typical flow fields in a side cavity. Figure 2 shows a typical sketch of a rectangular side cavity, where the dead zone like flow is generated.

1.2 Dead Zone at the downstream of encroached width in a open channel

In Bangladesh, the typical river encroachment means the earth filling of a portion of river course along the bank and pushing of river bank towards the center of river. Downstream of the fill, it creates a sudden enlarged portion along the river side. Such sudden enlarged zone due to width encroachment is mainly observed in small rivers running through the cities or towns. Such filling may be continuous along the stream or discontinuous.

This type of encroachment causes the reduction of channel cross-section, and thus the conveyance capacity of the river. It also causes the morphological changes of the river course; scouring occurred at the encroached section and silting or deposition of sediment are observed at the enlarged area. At the lee of the encroachment where the river suddenly enlarged, dead-zone like area is developed. Since the dead zone is a low velocity region, the sediment carried by the stream get deposited in that region. Therefore the downstream of the obstruction (earth fill) gradually becomes shallow compared to water depth at mainstream. Fig. 3 shows the definition sketch of open channel with sudden enlargement. The typical line of flow separation and dead zone is indicated in the figure. Fig.4 shows an example of river encroachment by earth filling in river in Bangladesh. Figure 4(a) shows that the vegetation is grown in the shallow depth region downstream of a obstruction in the river, and Fig. 4(b) shows the encroached is river width due to sand filling inside the river along the bank.

In this paper, the unsteady flow fields in a rectangular side cavity and that of sudden enlarged zone are simulated by unsteady RANS to investigate the characteristics of unsteady flow behaviour in a dead zone.

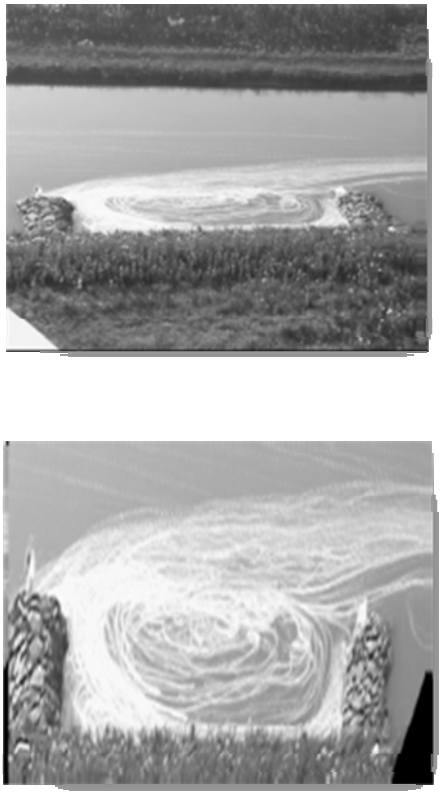

Figure 1. An example of flow behavior in rectangular side cavity (Muto et al., 2002)

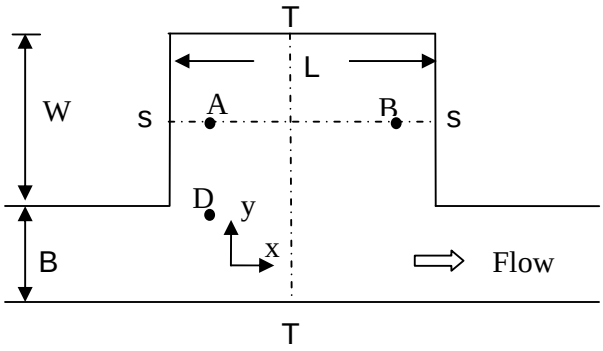

Figure 2. Sketch of the flow domain with rectangular side cavity (L=length of the cavity, W=width of the cavity, B= width of the main channel)

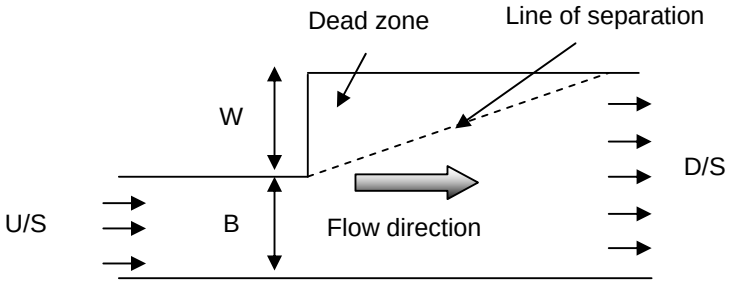

Figure 3. Definition sketch of open channel with sudden enlargement (B=Encroached width, W=Enlargement in width)

(a) Mayur River in Khulna (b) Balu River in Dhaka

Figure 4. Typical River encroachment in two city rivers in Bangladesh

2. Numerical model and simulation details

2.1 Non-linear k–ε Model in 3D Curvilinear Coordinate

The 3D flow equations in a *k–ε* model for an unsteady incompressible flow with contra-variant components of velocity vectors on a curvilinear coordinate system can be written as follows.

Continuity Equation:

$$\frac{1}{\sqrt{g}}\frac{\partial V^{\alpha}\sqrt{g}}{\partial \xi^{\alpha}} = 0 \tag{1}$$

Momentum equation:

$$\frac{\partial V^{i}}{\partial t} + \nabla_j\left[V^{i}(V^{j} - W^{j})\right] + V^{i}\nabla_j W^{j} + V^{j}\nabla_j W^{i} = F^{i} - \frac{1}{\rho}g^{ij}\nabla_j p + \nabla_j\left[-\overline{v^{i}v^{j}}\right] + 2\nu\nabla_j e^{ij} \tag{2}$$

k-equation:

$$\frac{\partial k}{\partial t}+\nabla_j\left[k(V^j-W^j)\right]+k\nabla_j W^j=-g_{il}\overline{v^l v^j}\nabla_j V^i-\varepsilon+\nabla_j\left\{\left(\frac{D_t}{\sigma_k}+\nu\right)g^{ij}\nabla_i k\right\}$$

(3)

ε-equation:

$$\frac{\partial \varepsilon}{\partial t}+\nabla_j\left[\varepsilon(V^j-W^j)\right]+\varepsilon\nabla_j W^j=-C_{\varepsilon 1}\frac{\varepsilon}{k}g_{il}\overline{v^l v^j}\nabla_j V^i-C_{\varepsilon 2}\frac{\varepsilon^2}{k}+\nabla_j\left\{\left(\frac{D_t}{\sigma_k}+\nu\right)g^{ij}\nabla_i \varepsilon\right\} \quad (4)$$

Here, V^j is the contra-variant component of velocity vector of the flow and W^j is that of the grid motion. g_{ij} and g^{ij} are covariant and contra-variant component of metric tensor. The covariant derivative is defined as

$$\nabla_i A^k=\frac{\partial A^k}{\partial \xi^i}+A^j\Gamma_{ij}\ ,\ \Gamma_{ij}{}^k=\begin{Bmatrix}k\\ij\end{Bmatrix}=\frac{1}{2}g^{km}\left(\frac{\partial g_{jm}}{\partial \xi^i}+\frac{\partial g_{im}}{\partial \xi^j}-\frac{\partial g_{ij}}{\partial \xi^m}\right)=\frac{\partial \xi^k}{\partial x^p}\frac{\partial^2 x^p}{\partial \xi^i\partial \xi^j} \quad (5)$$

here, $\Gamma_{ij}{}^k$ is the Christoffed symbol.

The constitutive equation for 2nd-order non-linear k–ε model used in this study is as follows

$$-\overline{v^i v^j}=D_t S^{ij}-\frac{2}{3}k\delta^i_s g^{sj}-\frac{k}{\varepsilon}D_t\left[\alpha_1 Q_1+\alpha_2 Q_2+\alpha_3 Q_3\right]$$

$$D_t=C_\mu\frac{k^2}{\varepsilon} \quad (6)$$

here,

$$Q_1=S^{i\alpha}g_{\alpha l}\Omega^{lj}+S^{j\beta}g_{\beta l}\Omega^{li}\ ,\ Q_2=S^{i\alpha}g_{\alpha l}S^{lj}-\frac{1}{3}S^{k\alpha}g_{\alpha m}S^{m\beta}g_{\beta k}\delta^i_l g^{lj}\ ,\ Q_3=\Omega^{i\alpha}g_{\alpha l}\Omega^{lj}-\frac{1}{3}\Omega^{k\alpha}g_{\alpha m}\Omega^{m\beta}g_{\beta k}\delta^i_l g^{lj} \quad (7)$$

Strain and rotation tensors are defined as

$$S^{ij}=g^{j\alpha}\nabla_\alpha V^i+g^{i\alpha}\nabla_\alpha V^j\ ,$$

$$\Omega^{ij}=g^{j\alpha}\nabla_\alpha V^i-g^{i\alpha}\nabla_\alpha V^j \quad (8)$$

Considering the coefficients of non-linear terms as a function of strain and rotation parameters, their values can be determined as follows

$$\alpha_1=-0.1325f_M\ ,\ \alpha_2=0.0675f_M\ ,$$

$$\alpha_3=-0.0675f_M\ ,\ f_M=\frac{1}{1+m_{ds}S^2+m_{d\Omega}\Omega^2} \quad (9)$$

Here, the functional form of c_μ is assumed as

$$c_\mu=\frac{c_{\mu o}\ (1+c_{ns}S^2+c_{n\Omega}\Omega^2)}{1+c_{ds}S^2+c_{d\Omega}\Omega^2+c_{ds\Omega}S\Omega+c_{ds1}S^4+c_{d\Omega 1}\Omega^4+c_{ds\Omega 1}S^2\Omega^2} \quad (10)$$

Here, the strain and rotation parameters are defined as

$$S = \frac{k}{\varepsilon}\sqrt{\frac{1}{2}S^{i\alpha}g_{\alpha j}S^{j\beta}g_{\beta i}}\ ,\ \ \Omega = \frac{k}{\varepsilon}\sqrt{\frac{1}{2}\Omega^{i\alpha}g_{\alpha j}\Omega^{j\beta}g_{\beta i}} \tag{11}$$

The model constants are given in Table 1(for details please see in Kimura et al., 2009 and Ali, 2008).

Table 1
Values for the coefficients of c_μ and c_β

Model const.	$c_{\mu 0}$	c_{ns}	$c_{n\Omega}$	c_{ds}	$c_{ds\Omega}$	$c_{d\Omega}$
values	0.09	0.005	0.0068	0.008	-0.003	0.004
	c_{ds1}	$c_{d\Omega 1}$	$c_{ds\Omega 1}$	m_{ds}	$m_{d\Omega}$	
	0.00005	0.00005	0.00025	0.01	0.003	

2.2 Computational schemes and flow domain

The governing equations for mean velocities and turbulent flows are discretized with the finite volume method based on full staggered boundary fitted coordinate system. For the momentum equation, convective and diffusive fluxes are approximated with Quick and central difference schemes respectively. The hybrid central upwind scheme is used for the k and ε equations. Time advancement is achieved by Adam-Bashforth scheme of second-order accuracy in each equation. The basic equations are discretized as fully explicit forms and solved successively with the time increment in step by step. The pressure field is solved using iterative procedure at each time step. The free surface elevation is solved by continuity equation integrated over the control volume of the surface layer. The wall functions are employed as the wall boundary conditions for k and ε. The frictions near the bed and side walls are estimated by log-law. An inflow velocity is prescribed in upstream end, and fixed depth with zero velocity gradient is used as boundary condition at downstream end of the flow domain.

The numerical simulations for 3-D unsteady flows are performed for three cases: two cases (C1 and C2) for open channel with rectangular side cavity and one case (E1) for sudden enlarged zone. The hydraulic conditions for Case C1 and C2 are shown in Table 2. Case C1 is simulated under the same conditions of laboratory experiments conducted by Kimura and Hosoda (1997). Case C2 is simulated to investigate the effect of length to width ratio (L/W) on the flow field. The plan view of the computational domain of side cavity is shown in Fig. 2, and that of sudden enlarged channel is shown in Fig. 3. The flow domain consists of 76 grids in longitudinal (stream-wise, *x)*, 42 in transverse (width-wise, *y*) and 10 in perpendicular to bed (depth-wise, *z)* directions. The simulated results are presented in the following two sections.

Table 2
Hydraulic parameters for the simulations of open channel flows with a rectangular side cavity

Case no.	B (cm)	L (cm)	W (cm)	L/W ratio	Q_0 (cm^3/s)	ho (cm)	Fr no.	Bottom slope	Δt (sec)
C1	10	22.5	15	1.5	747.0	2.02	0.83	1/500	0.0001
C2	10	45	15	3	747.0	2.02	0.83	1/500	0.0001

Table 3
Hydraulic parameters for the simulations of open channel flows with a sudden enlarged zone

Case no.	B (cm)	L (cm)	W (cm)	L/W ratio	Q_0 (cm^3/s)	ho (cm)	Fr no.	Bottom slope	Δt (sec)
E1	10	135	15	9	255	1.00	0.81	1/1000	0.0001

3. Flow characteristics in a side cavity

3.1 Time averaged flow properties

The unsteady flow in a dead zone is characterized by three important flow criteria: the circulation and oscillation inside the dead zone, and the coherent vortices at the interface of main stream and dead zone. However, the time averaged flow does not show instability characteristics. Figure 5 shows the time averaged (averaging for 10 sec) velocity vector, which mainly characterized by the circulation inside the dead zone. The simulated vector field and the circulation pattern are very similar to the previous experimental and 2D numerical studies (Kimura and Hosoda, 1997; Takemoto et al., 1984).

Figure 6 shows the time averaged profile of stream-wise velocity (u) along the transverse cross-section at centerline of dead zone (the section is shown in Fig. 2 as T-T). The comparison of simulated result with experiment shows good agreement.

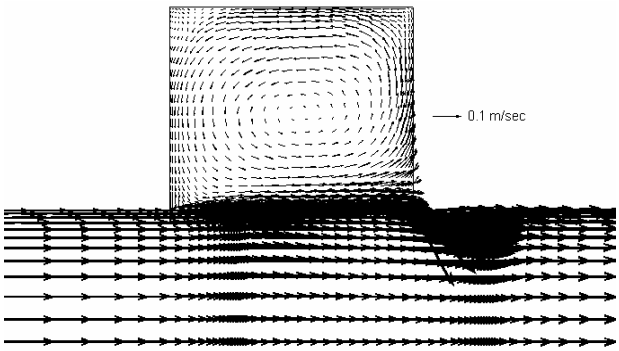

Figure 5. Time averaged velocity vectors

3.2 Temporal variation of flows

The formation of instability vortices at the interface of main channel and dead-zone and its interaction with dead-zone circulation can be described by considering the temporal change of velocity vectors as well as the variations in water depth as shown in Fig. 7. Due to space limitation, only two vector plots and corresponding water depth distributions are shown in the figure for t=54.4 and 54.8 sec. It can be noted that the period of instability vortex for this flow is found about 0.8 sec. The deviation of velocity vectors from the main circulation near the interface shows the position of instability vortices. It is found that the instability vortex observed at upstream corner of interface moves downstream with gradual amplification with time, and the process continues repeatedly with a constant periodic interval. The figure shows that the instability vortex at upstream of dead zone interface for t=54.4 sec is moved downward at t=54.8 sec with a formation of new vortex at upstream corner.

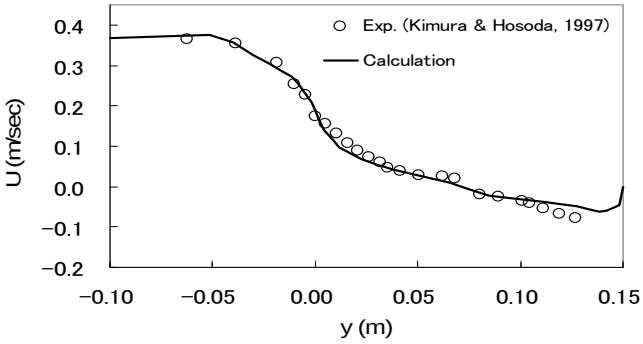

Figure 6. Comparison of time averaged velocity profile along T-T Section of Fig 2.

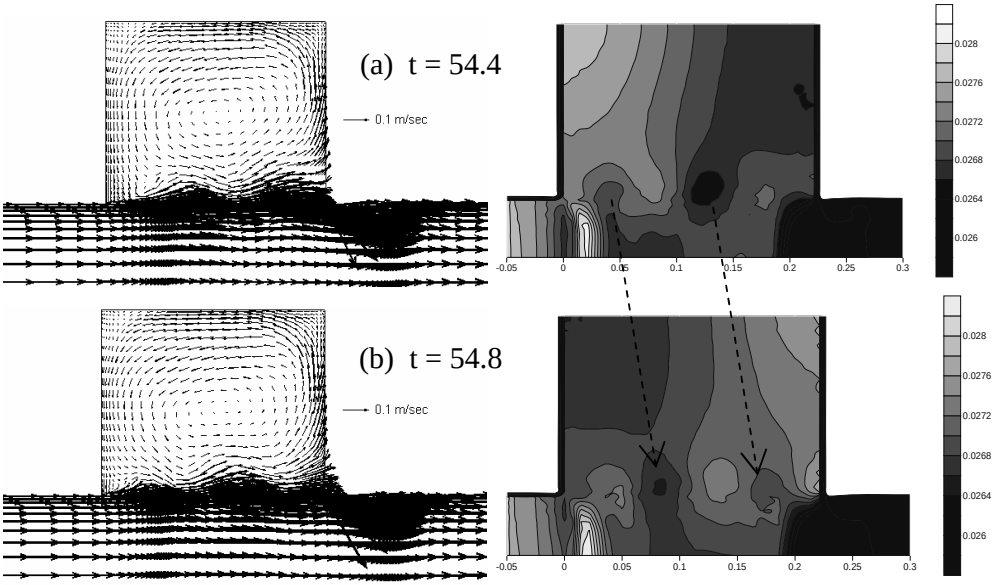

Figure 7. Instantaneous velocity vectors (left side) and water depth contours (right side) at two different times with 0.4 sec interval.

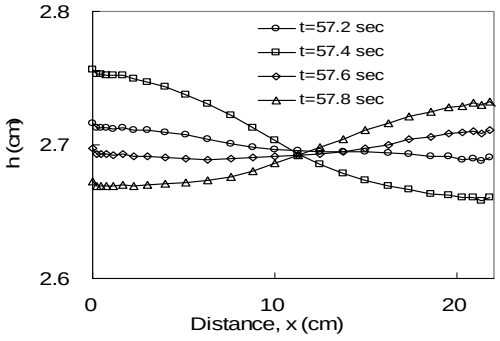

Figure 8. Oscillation of water surface inside the dead-zone (S-S section).

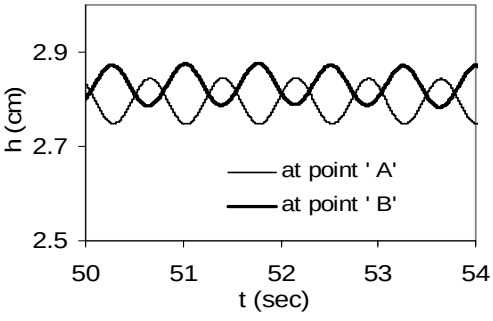

Figure 9. Temporal variation of water surface at point A and B.

The temporal variations of water surface distribution demonstrate two important phenomena: one is seiche inside the dead-zone, and another is depression of water surface at the center of instability vortices. The depression in the free surface moves downward with time along the interface, as observed in the movement of large vortices in vector plots. In the present flow domain two to three depressions in water surface can be seen in an instantaneous flow field. Since, the vortices at the upstream corner are premature and those near the downstream corner are decayed due to merging with main circulation, the large vortices at the middle part of the interface are most matured and show highest depression in the surface.

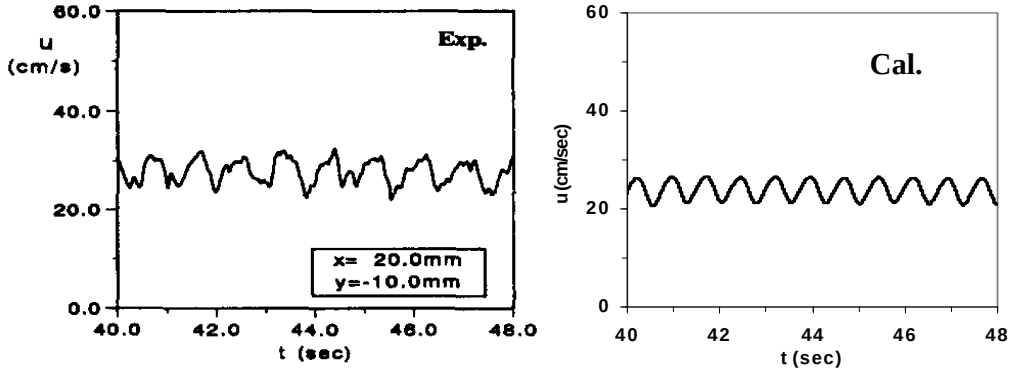

Figure 10. Temporal variations in stream-wise velocity (u) at point D.

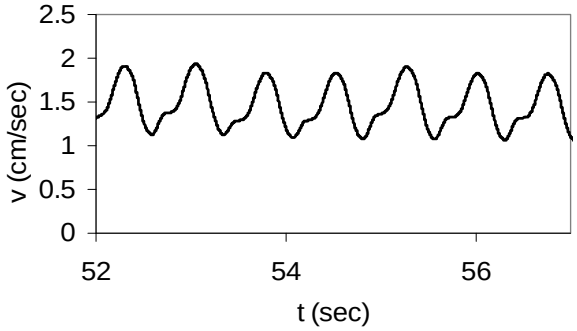

Figure 11. Temporal variation of transverse-velocity component (v) at the interface (x =5 cm).

The second important phenomenon demonstrated by the contours is the oscillation inside the dead zone. If we look the water surface distribution inside the dead zone, Fig. 7(a) shows minimum depth at downstream end and maximum depth in upstream end of dead zone; on the other hand, Fig. 7(b) shows reverse phenomena. A periodic change in the depth difference between upstream and down stream end of dead zone indicates the existence of oscillation in the cavity.

This oscillation of water surface is clearly demonstrated in Figs. 8 and 9. In Fig. 8, the spatial water depth distribution in the dead zone along the section S-S (location of section is shown in Fig. 2) is shown for different time intervals. It explains that the node of oscillation, that contains the lowest seiche mode with a direction parallel to the main flow, is located near the center of the circulation. The wavelength of the oscillation is about twice the dead-zone length. Comparing with Fig. 7, it is observed that the depth variation inside the dead zone is mainly due to the seiche, and near the interface it is governed by the instability vortices.

Figure 10 shows the calculated results for temporal free surface oscillation at point A and B. The period of oscillation is found as 0.75 sec, which is slightly smaller than the experimentally observed value of 0.87 sec. The calculated magnitude of velocity variation is well agreed with experiment. The period of oscillation in the temporal changes of u-velocity is found same with the periodic oscillation of water surface. The temporal change of transverse velocity component (v) at a point on the interface (x =5 cm, y =0) is shown in Fig. 11. It is observed that, each cycles of temporal velocity variations consists two components of oscillations. The long one is due to seiche and has a time period of 0.75 sec. The period of short oscillation component is about 0.15-0.25 sec, which is caused by the instability vortices. This phenomenon is also reported in previous experimental observations.

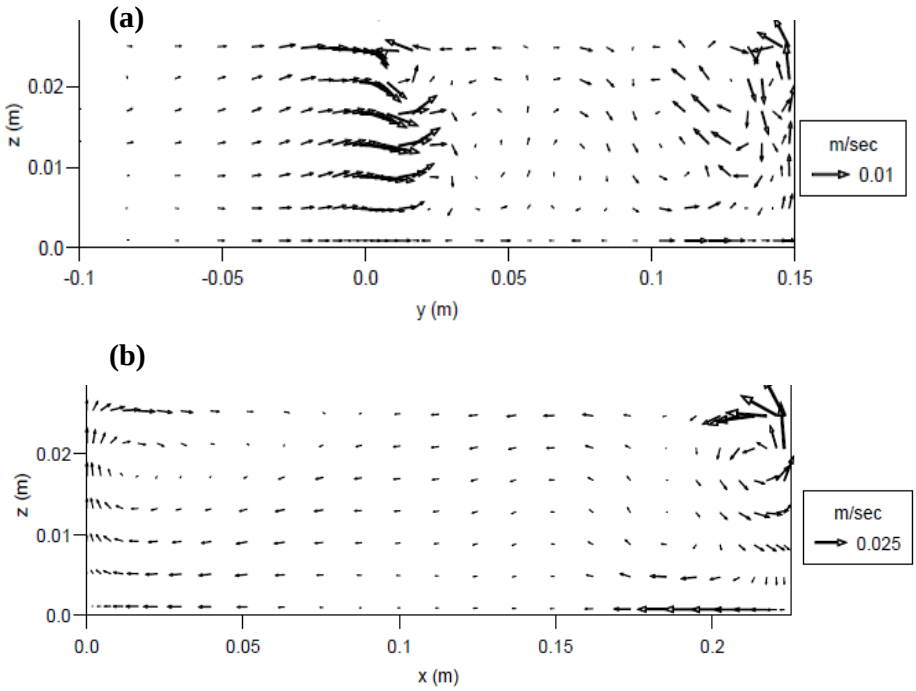

Figure 12. Secondary currents along (a) T-T section and (b) S-S section

3.3 Behaviour of secondary currents

Although the depth of the flow is small, strong secondary currents are found to be generated at inside the dead zone as well as near the interface area. Figure 12 shows the pattern of secondary current at T-T and S-S section in the time averaged flow field. The sectional locations are shown in Fig. 2. In the figure, Surface and corner circulation cells near the boundaries of dead-zone are clearly depicted. Although, several circulation cells are observed at the middle of dead-zone in T-T section with the size equal to the depth, the circulation cells near the interface and at the boundary region are found to be much stronger and seem to be a general feature of the dead zone flow. The flow exchange between main-channel and dead zone can be seen in the sections of an instantaneous flow field as observed in the plan view of flow vectors in Fig. 7.

3.4 Effect of aspect ratio (L/W) of the cavity

For case C2, the ratio of the dimensions of the cavity is taken as L/W=3 to identify the change in flow behavior due to change in length. The simulated result of vector flow field shows that, with increasing the length of the cavity the circulation pattern and their numbers are changed along with velocity magnitude. In previous cases, only one circulation was observed, but in case 2 (Fig. 13) there are about three circulations, among them two are the main circulations and one is at left corner which is called corner vortex. The exchange of flow between mainstream and dead zone is very prominent comparing with the previous case. Figure 14 shows the fluctuation of water surface in the simulated flow field. The deep colour shows low depth of channel and the light colour shows higher depth in the contour map. The figure indicates that the water surface is highly fluctuating along the interface. Although the circulation pattern inside the cavity for case C2 is quite different than that of case C1, the fluctuation pattern in water surface is observed to be similar.

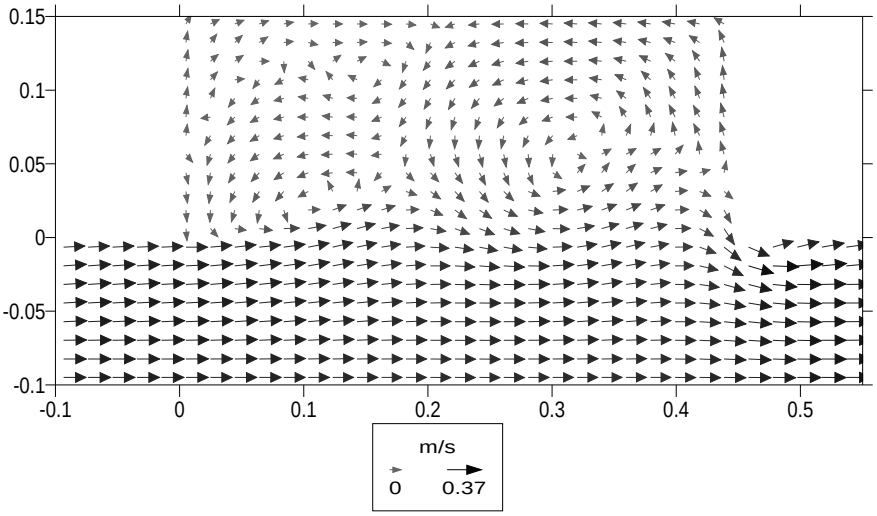

Figure 13. Instantaneous velocity vectors for case C2

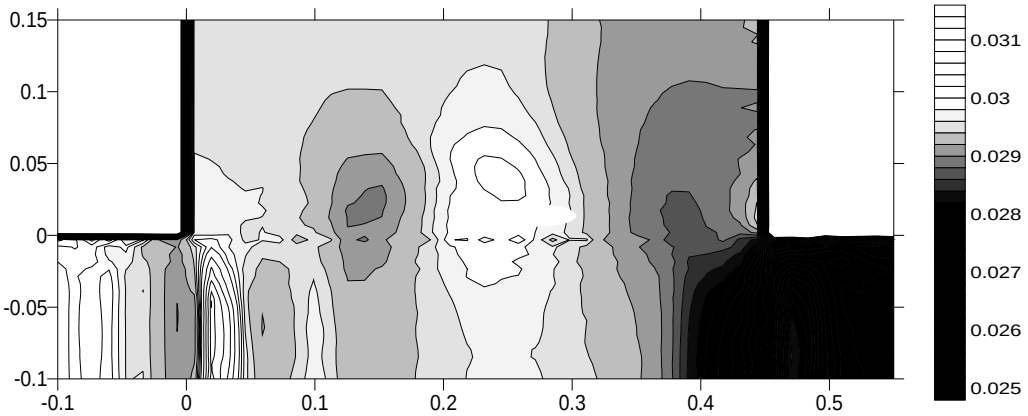

Figure 14. Fluctuation in water surface in the simulated flow field for case C2

4. Flow characteristics in a sudden enlarged zone

The difference between flow domains of a sudden enlarged zone with that of side cavity is only the downstream boundary. In a cavity the downstream is closed and water cannot flow freely but to exchange the momentum in lateral direction with the mainstream flow. On the other hand, for the open channel with sudden enlargement, although the upstream arrangement of flow domain is same as the cavity flow, the flow in the enlarged zone has the freedom to flow towards downstream in longitudinal direction. Due to this free downstream, the simulated flow field in the sudden enlarged zone is significantly different than that of open channel flows with side cavity. The simulated flow field of open channel flow with sudden enlarged zone for case E1 is shown in Fig. 15. Only one main circulation is observed in the dead zone of the enlarged portion of the channel. The main flow is observed to be deflected to wards the enlargement (left side). At the end of the main circulations a small circulation formed at the opposite site of the enlargement (right side) due to the movement of flow towards left side. After that the velocity vector is observed to be approached to the uniform flow. The contour of stream-wise velocity component is shown in Fig. 16. White colour shows the high velocity region and the blackish indicates the lower velocity region. The deep black area is the negative velocity region. The path of high velocity stream is clearly observed in the contour. Two circulation regions that contain negative stream-wise velocity are also easily distinguishable from main stream flow. Figure 17 shows the fluctuation of water surace in the simulated flow field. The deep colour shows low depth of channel and the light colour shows higher depth in the contour map. The figure indicates that the water surface is highly fluctuating along the interface. The water surface is observed to be depressed in the circulation with lowest depth at the center of the circulation. Since the circulation pattern in dead zone for case C1 and C2 is different than that of case E1, the fluctuation pattern in water surface is also observed to be different.

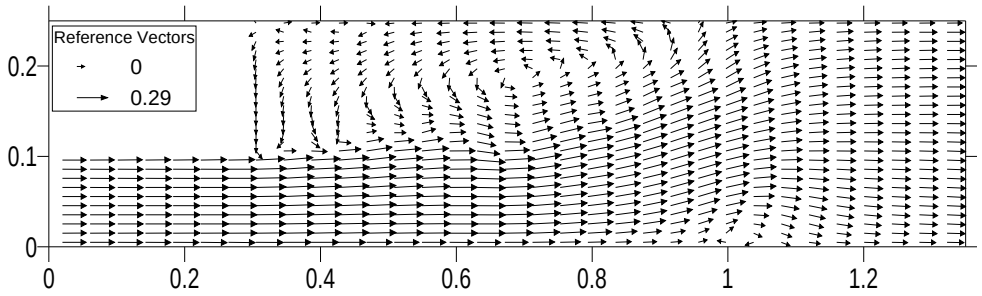

Figure 15. Instantaneous velocity vectors for case E1.

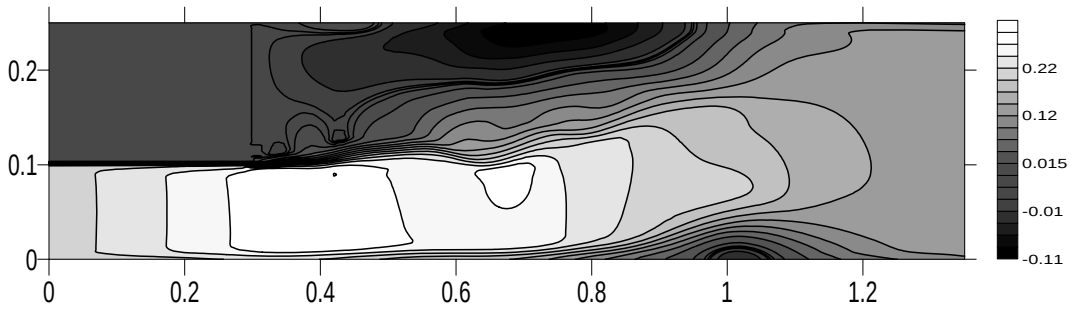

Figure 16. Contour of stream-wise velocity (U-velocity component in m/s) for case E1.

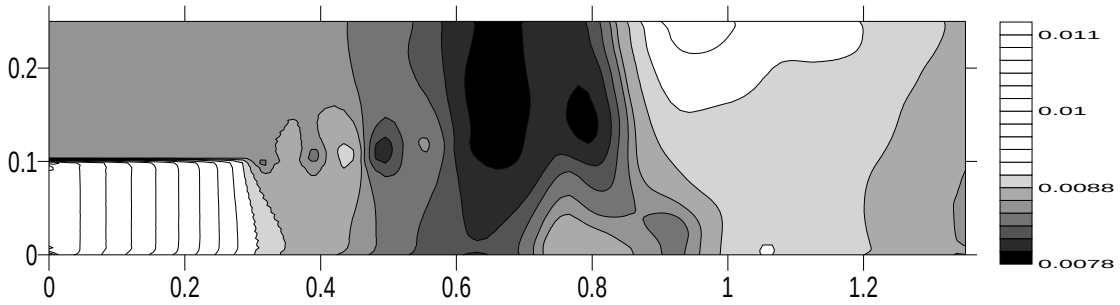

Figure 17. Fluctuation in water surface in the simulated flow field for case E1.

5. Conclusions

The flow fields in an open channel with two types of dead zone have been investigated by three-dimensional unsteady RANS computations: one is rectangular side cavity and another one is the dead zone created at the downstream of channel with width encroachment (i.e. sudden enlarged zone). The time averaged flow properties and temporal change of velocity profiles are well compared with previous experimental results. Based on the results following conclusions are made.

a) It is found that the flow in the side cavity is characterized by three types of flow phenomena: the circulation inside the dead-zone, periodic coherent vortices at the interface of main stream and dead zone, and the water surface oscillation inside the dead zone. In this study all these characteristics are successfully reproduced by numerical simulation.

b) The temporal variation of water surface shows a depressed water depth at the center of coherent vortices. This hollow of the free surface moves downward with time along the interface, as observed in the movement of large vortices in vector plots. In the calculated result, a periodic change in depth difference between upstream and downstream end of dead zone indicates the existence of oscillation in the cavity. The period of oscillation is found same as that of instability vortex. Although the depth of the flow is small, strong secondary currents are found to be generated at inside the dead zone as well as near the interface area.

c) An exchange of flow between mainstream and dead zone is observed is observed. Due to the formation of circulation in the dead zone, the velocity is very small compared to main stream, and the velocity at the center of circulation is zero. For length to width ratio of the cavity as 1.5 (L/W=1.5), the center of the circulation is found to be situated at the middle of the cavity in both the directions.

d) with increasing the length of the cavity, the circulation pattern and their numbers are changed along with velocity magnitude. In previous case, only one circulation was observed, but in the case with higher length to width ratio of the cavity (L/W=3), there are about two main circulations in the cavity, the first one is smaller than the second one due to the suppression by the prominent corner vortex. In this case the exchange of flow between mainstream and dead zone is very prominent compared to previous case.

e) For the open channel with sudden enlargement, although the upstream arrangement of flow domain is same as the cavity flow, the flow in the enlarged zone has the freedom to flow towards downstream in longitudinal direction. Due to this free downstream, the simulated flow field in the sudden enlarged zone is significantly different than that of open channel flows with side cavity. Only one main circulation is observed in the dead zone of the enlarged portion of the channel. The main flow is observed to be deflected to wards the enlargement (left side). At the end of the main circulations a small circulation formed at the opposite site of the enlargement (right side) due to the movement of flow towards left side. The water depth at the centre of circulation is low compared to surroundings.

Finally, it can be concluded that the dead zone is a low velocity region, and due to this low velocity the sediments carried by the stream may deposit there easily to form shallow depth region. The effect of width encroachment due to earth filling or construction of any obstruction extending inside the river also creates dead zone that finally may filled up by sediments. Beside the academic research interests, the present study contributes to understand the development, extent and behaviour of flows in a dead zone for proper management of river system and other water courses.

References

Ali, M. S. (2008). Model refinement of unsteady RANS and its practical applications in the field of hydraulic engineering. PhD Thesis, Kyoto University, Japan.

Kimura, I. and Hosoda, T. (1997). Fundamental properties of flows in open channels with dead zone. J. Hydr. Engg., ASCE, Vol. 123, pp. 98-107.

Kimura, I., Uittewaal, W. S. J., Hosoda, T. and Ali, M. S.(2009). Non-linear RANS computations of shallow grid turbulence. Journal of Hydraulic Engineering, ASCE, Vol. 135, No. 2, pp. 118-131.

Mizumura, S.Y. and Yamasaka, C. J. (2002). Flow in open channel embayment. J. Hydr. Engg., ASCE, Vol. 128, pp. 1098-1101.

Muto, Y., Baba, Y., Aya, S. (2002). Velocity measurements in open channel flow with rectangular embayments formed by spar dykes. Annuals of Disas. Prev. Res. Inst., Kyoto Univ., No. 45B-2.

Takemoto, Y., Yamabe, H., Abe, Y. and Naitou, H. (1984). On the third upwind finite difference scheme in numerical analysis for initial value problem. Res. Rep., Inst. Plasma Phys., Nagoya University, IPPJ-693, Nagoya, Japan.